Mapping surface plasmons at the nanometre scale with an electron beam

To cite this article: Michel Bosman *et al* 2007 *Nanotechnology* **18** 165505

IOP PUBLISHING NANOTECHNOLOGY
Nanotechnology **18** (2007) 165505 (5pp) doi:10.1088/0957-4484/18/16/165505

Mapping surface plasmons at the nanometre scale with an electron beam

Michel Bosman[1], **Vicki J Keast**[2], **Masashi Watanabe**[3], **Abbas I Maaroof**[4] **and Michael B Cortie**[4]

[1] Electron Microscope Unit, The University of Sydney, NSW 2006, Australia
[2] School of Mathematical and Physical Sciences, The University of Newcastle, Callaghan NSW 2308, Australia
[3] Department of Materials Science and Engineering, Lehigh University, Bethlehem, PA 18015, USA
[4] Institute for Nanotechnology, University of Technology, Sydney, NSW 2007, Australia

E-mail: vicki.keast@newcastle.edu.au

Received 2 February 2007
Published 23 March 2007
Online at stacks.iop.org/Nano/18/165505

Abstract
The optical response from metal nanoparticles and nanostructures is dominated by surface plasmon generation and is critically dependent on the local structure and geometry. Electron energy-loss spectroscopy (EELS), combined with recent developments in spectrum imaging and data processing, has been used to observe the energy and distribution of surface plasmons excited by fast electrons. The energy of the plasmon responses is consistent with the optical response and with calculations. For gold and silver rods and ellipsoids, longitudinal, transverse and distinct cluster modes were readily identified and mapped. The spatial resolution of the presented maps is one order of magnitude better than that achievable with scanning near-field optical microscopy (SNOM)-based techniques.

(Some figures in this article are in colour only in the electronic version)

1. Introduction

Surface plasmons in coinage metal nanostructures are attracting a considerable amount of attention for applications such as: single-molecule detection with surface-enhanced Raman spectroscopy (SERS) [1, 2], the sub-wavelength manipulation of light [3–5] or medical treatment of tumours [6].

A surface plasmon is a collective oscillation of the conduction electrons that propagates along a surface and is generated by an external electric field. Alternatively, for small objects such as small spheres and rods, we can describe the surface plasmon as a polarization of the object. Surface plasmons are usually generated by the electric field component of an irradiating electromagnetic wave and their effect on the optical response of the materials is the main source of interest for applications. However, it is also possible to excite a surface plasmon with high energy electrons, as found in a transmission electron microscope (TEM) or scanning TEM (STEM).

The surface plasmon will have a resonant oscillation frequency and energy that is determined by the local size, shape and dielectric environment of the metal surface. Being able to directly correlate the local geometry with the surface plasmon energy is fundamental to our understanding of the optical response of metal nanostructures.

Most optical spectroscopic methods will not be able to provide this direct correlation for nanostructured metals. The sampling volume of these techniques is much larger than the local variations in surface geometry and the measured response will be an average over the area sampled. Alternative techniques with a spatial resolution of the order of the size of the nanostructures must be used. The most widely used method for spatially resolved surface plasmon detection is the scanning near-field optical microscope (SNOM or NSOM). This technique has been used to map the surface plasmon intensity on nanostructured gold [7–9] and can achieve a resolution of 20–30 nm. It has been shown that the spatial resolution of the measurements can be improved to ∼10 nm by exciting the surface plasmons with a scanning tunnelling microscope instead of a small aperture light source [10]. More recently SNOM has been used to measure the enhanced fields of nanoparticle dimers and trimers [11, 12].

As an alternative, electron energy-loss spectroscopy (EELS) in the STEM has been used for decades to detect surface plasmons, usually by placing the electron beam close to the metal surface and measuring the energy lost by the beam. Unlike light, an electron beam can excite surface plasmons from planar surfaces as well as bulk plasmons. EELS has been used to detect plasmons from, for example, single spheres [13], coupled spheres [14] and supported spheres [15].

In this paper we will show that by implementing new techniques in EEL spectrum imaging and spectral processing [16], it is possible to map the surface plasmon response with a spatial resolution of about one order of magnitude better than that achieved with SNOM. Such a resolution enhancement allows the detailed study of the relationship between the size and shape of metal nanostructures and their surface plasmon energy and intensity. Examples from gold and silver particles in a variety of shapes will be given.

2. Experimental details

The gold nanospheres were prepared by the citrate-reduction route. All glassware used was cleaned in aqua regia (three parts of concentrated HCl plus to one part of concentrated HNO_3) before use. $HAuCl_4{\cdot}3H_2O$ (1 mM) was used as a starting solution. This was transferred to a 250 ml conical flask for heating and stirred vigorously. When the temperature reached 90 °C, 10 ml of 38.8 mM sodium citrate was quickly added. A blue colour immediately developed which changed shortly thereafter to the well-known deep burgundy of gold nanosphere sols. Heating continued for another 15 min after which the solution was removed from the heater and stirred for a further 15 min. The sol was stored at 4 °C.

The gold nanorods were prepared by a modification of the seed-mediated growth method [17, 18]. A 'seed' solution of spherical gold nuclei was first prepared by mixing 0.10 ml of 0.02 M KBH_4 with 10.0 ml of an aqueous solution containing 0.5 mM $HAuCl_4$ and 0.2 M cetyl-trimethyl-ammonium bromide (CTAB). After vigorous stirring for 30 min 12 μl of this 'seed' solution was added to a 'growth' solution at room temperature. The latter was prepared by adding 0.10 ml 0.10 M L-ascorbic acid to 10.0 ml aqueous solution containing 0.2 M CTAB, 0.5 mM $HAuCl_4$, and 0.1 ml of 10 mM $AgNO_3$ with stirring. The formation of gold nanorods proceeded over a period of several tens of minutes, and was associated with the development of a purple to blue colour in the growth solution. Large spherical particles could be removed by low speed (2000 rpm) centrifugation. Following this, 10 ml of colloid was centrifuged at 13 000 rpm for 25 min, and the supernatant was carefully tipped off. The pellet was mixed with 10 ml of double-distilled water and the washing procedure was repeated twice to remove surplus CTAB. The final colloid contains 50–100 times the concentration of gold nanorods in the original solution with approximately 2 mM of CTAB left. The concentrated gold nanorods colloid was stored in dark, ambient conditions, and used over the course of the next several weeks.

Arbitrary silver ellipsoids have been obtained by using a nanosphere lithography (NSL) method [19]. A suspension of polystyrene spheres of diameters 100 nm was obtained from Spherotech Inc. and then diluted by a 1:400 solution of the surfactant Triton X-100 in methanol. The respective dilution factors were 20 μl of nanoparticles and 100 μl of the surfactant and methanol. After dilution the nanosphere suspensions were spin-coated onto NaCl substrate. The spin coater (Headway Research Inc.) was operated at 3000 rpm for 30 s. Then, a thin film of 30 nm silver was deposited on the sample using DC magnetron sputtering. The sputtering targets of Ag were 99.999% pure discs (50 mm diameter), placed 150 mm away from the substrate. The base pressure was better than $\sim 10^6$ Torr, while sputtering was carried out in the presence of flowing Ar, at a pressure of 2 mTorr. The nanospheres were removed by sonicating the substrate in CH_2Cl_2 for 5 min. The final specimen consisted of a variety of spherical, near-spherical and ellipsoidal shapes.

For all gold particles, a drop of the solution containing the particles was deposited on a thin mica ($\sim$20 nm) support. Mica was chosen as it is easily cleaved into thin films and, because of its large bandgap, has no features in the EELS spectrum that obscure the signal from the small gold particles. A standard carbon support film was used for the silver particles; their higher plasmon energy and intensity did not necessitate the use of mica as a support film.

The EELS maps were acquired using a VG HB601UX STEM with a cold field emission gun (CFEG) and a Gatan Enfina EEL spectrometer. The incident electron beam has an energy of 100 keV. A lower than typical extraction voltage was used for the CFEG in order to improve the spectral resolution from the usual value of 0.40 eV down to 0.25 eV (measured as the full width at half maximum of the zero-loss peak). To compensate for the diminished beam current at low extraction volts, an electron beam with a relatively large diameter of 2–3 nm was used; less than 1 nm is typical for this instrument. This operation does not significantly degrade the observed spatial resolution because the impact parameter for the electron–electron interaction dominates at these low energy losses [20].

For the spectrum imaging technique, the electron beam is scanned over the specimen in a rectangular raster of pixels and at each pixel an EEL spectrum is acquired [21]. From each of the individual spectra in the data set, the spectral features of interest can be extracted and mapped to visualize their spatial distribution. The acquisition time of the EEL spectrum images was reduced by on-chip binning in the CCD camera of the spectrometer. For the data presented here the acquisition time per spectrum was 2 ms.

Because of the short acquisition times for each pixel, the individual spectra that are obtained are relatively noisy, introducing inaccuracies when conventional processing methods are used. For this work, the spectrum images were analysed with principal component analysis (PCA), where all the spectra are analysed at once, instead of individually. As has been shown previously, such an approach is a very effective way to remove random noise from the spectra without the degradation of spectral resolution [16]. After the careful subtraction of a pre-measured zero-loss peak model from the individual spectra, the random noise was removed using PCA and a Gaussian was fitted to the surface plasmon peak using a non-linear least-squares fit routine. The amplitude of the Gaussian was then used to map the intensity of the surface plasmon, while the position of the Gaussian maximum

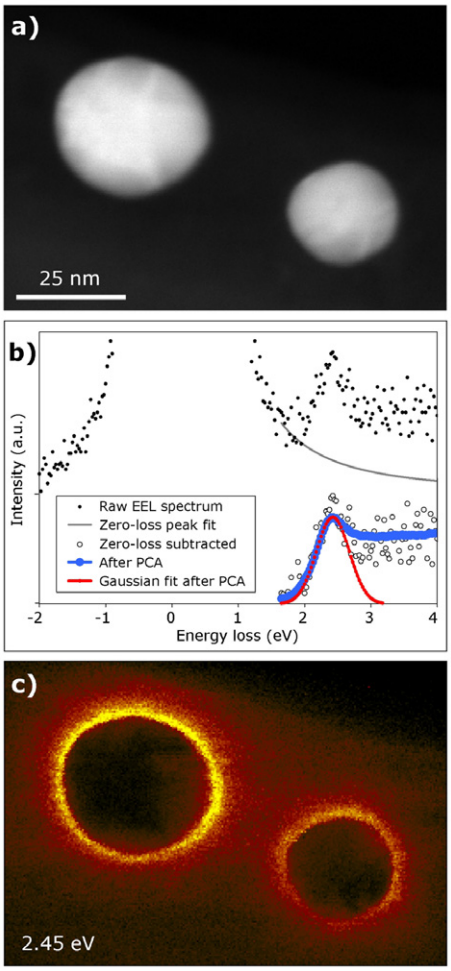

Figure 1. (a) Annular dark field image in the STEM of two gold spheres, 25 and 35 nm in size. (b) A typical spectrum from a single pixel of the map, showing the effect of: zero-loss peak subtraction, noise removal with PCA and Gaussian curve fitting to the surface plasmon peak. The last three curves were shifted down for clarity. (c) The corresponding map of the intensity of the surface plasmon at 2.45 eV ($\lambda = 506$ nm).

was used to determine the energy position of the surface plasmon. The width of the Gaussian should, in principle, provide information on the lifetime of the plasmon resonance. However, the energy resolution in these experiments was close to the expected plasmon peak widths [22] and conclusive plasmon lifetime measurements were therefore avoided. To enhance regression robustness, the width of the Gaussian fit was constrained to a constant value.

3. Results and discussion

Figure 1(a) shows an annular dark field (ADF) image of two gold spheres, 25 and 35 nm in size. Figure 1(b) shows one of the spectra from the map, before and after noise removal, and illustrates the Gaussian fitting procedure. In figure 1(c), the corresponding map of the surface plasmon intensity is shown. The energy of the surface plasmon is 2.45 ± 0.05 eV and is unchanged throughout the map, as we would expect for

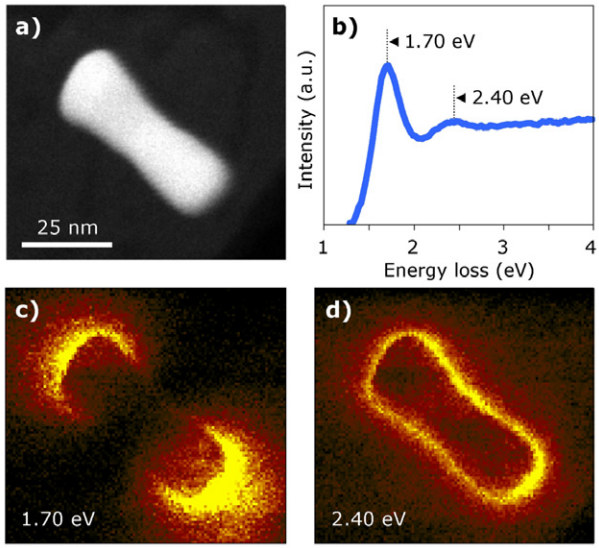

Figure 2. (a) Annular dark field STEM image of a gold nanorod. (b) The average spectrum (summation of all spectra in the spectrum image) from this rod, after zero-loss peak removal. (c) Map of the intensity of the plasmon resonance at 1.70 eV ($\lambda = 730$ nm). (d) Map of the intensity of the plasmon resonance at 2.40 eV ($\lambda = 517$ nm).

spherical particles of this size. This energy is consistent with Mie theory and previous optical measurements [23].

Figure 2(a) shows an ADF image of a gold nanorod with length, $l \approx 50$ nm and an aspect ratio of $R \approx 3.1$ (at the narrowest part). The summation of all spectra, after zero-loss peak subtraction, is shown in figure 2(b). Two distinct plasmon resonances are observed; one at 1.70 ± 0.05 eV and one at 2.40 ± 0.05 eV. The intensity distributions for these two modes are shown in figures 2(c) and (d) respectively. The energy of the plasmons is consistent with previous calculations based on ellipsoids with Gans' extension to Mie theory [22] and the maps show the intensity distribution of the longitudinal and transverse modes. When the electron beam passes the end of the rod the electric field is primarily directed along the long axis of the rod, which is equivalent to polarization of light along this direction. Calculations using the discrete dipole approximation (with DDSCAT [24]) on gold particles of this shape give an energy of 1.91 eV for the longitudinal resonance and 2.38 eV for the transverse resonance.

Figure 3(a) shows an ADF image of a cluster of three particles consisting of two nanorods aligned end to end and an adjacent cube-shaped particle that is in contact with one of the rods. In this multi-particle cluster, three distinct plasmon resonances were observed: at 1.20 ± 0.05 eV, 1.95 ± 0.05 eV and 2.40 ± 0.05 eV. The intensity of these three plasmons is plotted in figures 3(b), (c) and (d) respectively. These images indicate that the three modes can be identified as: the usual transverse mode (2.40 eV), a longitudinal mode for the whole cluster (1.20 eV) and a longitudinal mode for each rod (1.95 eV).

In figure 4(a), an ADF image of an ellipsoidal silver particle is shown; figure 4(b) shows examples of spectra from the three regions indicated. Silver has a strong, sharp bulk plasmon peak at 3.75 ± 0.05 eV and it dominates the EEL spectrum when the electron beam passes through the centre of

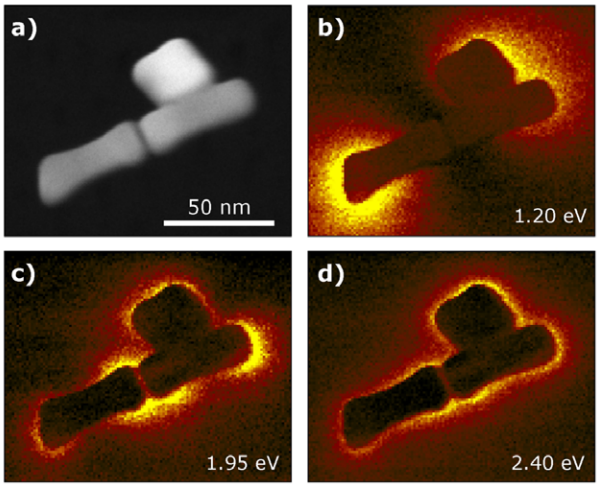

Figure 3. (a) Annular dark field STEM image of a cluster of three gold particles consisting of two nanorods aligned end to end and an adjacent cube-shaped particle. (b) Map of the plasmon intensity at 1.20 eV ($\lambda = 1033$ nm), showing the resonance mode of the whole cluster. (c) Map of the plasmon intensity at 1.95 eV ($\lambda = 636$ nm), showing the longitudinal mode for each rod. (d) Map of the plasmon intensity at 2.40 eV ($\lambda = 517$ nm), showing the transverse mode.

the particle. For this particle, there are two surface modes: the transverse mode at 3.45 ± 0.05 eV and the longitudinal mode at 2.45 ± 0.05 eV. The intensity distribution of these plasmon resonances are given in figures 4(c)–(e). To obtain the intensity distribution for the bulk plasmon it was first necessary to subtract the contribution from the 3.45 eV surface plasmon from each spectrum.

Although in both optical and EELS experiments a surface plasmon is generated, there are subtle differences in the excitation process. In the case of EELS for example, the incident electric field will not be spatially homogeneous throughout the particle/s and is critically dependent on the beam position, whereas it will be homogeneous when light is used to excite the surface plasmons. The time dependence of the incident electric field is quite different too in both cases, although the fast pulse of the electric field of the incident electron can be considered as a summation of frequency dependent electric field components. Finally, the calculations to go from the induced field to the extinction coefficient (for light) or to the energy-loss probability (for EELS) are quite different. For these reasons we may not expect precise agreement between the optical and EELS measurements. Surprisingly, despite there being a significant number of quantitative calculations of the optical response and, separately, of the EELS response, there have not been any publications connecting these two spectroscopies. However, we know that in the limit of the non-retarded case, for dipole excitation of small spherical particles, the optical extinction [25] and the energy-loss [26] are equivalent. A detailed reconciliation between surface plasmon measurements using light and electrons will be the subject of a future publication.

The observed intensity distribution for the plasmon response from individual particles bears a strong resemblance to calculations of the induced fields for optical excitation. This is not unexpected because the energy lost by the incident beam is determined by the induced electric field. However, given the differences between optical and electrical excitation discussed above, we should be cautious about making any

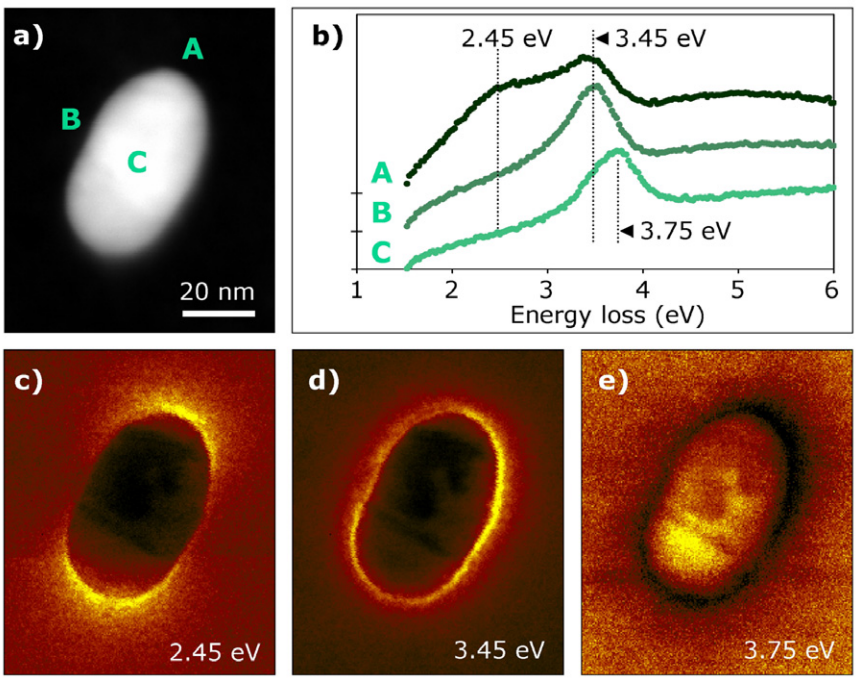

Figure 4. (a) Annular dark field STEM image of an ellipsoidal silver particle. (b) Spectra from the three regions indicated in (a). (c) Map of the plasmon intensity at 2.45 eV ($\lambda = 506$ nm), showing the longitudinal resonance mode. (d) Map of the plasmon intensity at 3.45 eV ($\lambda = 360$ nm), showing the transverse resonance mode. (e) Intensity map of the bulk plasmon resonance at 3.75 eV ($\lambda = 330$ nm). The intensity in the last map further than about 10 nm off the ellipsoid is caused by spectral noise.

quantitative comparisons, especially for multi-particle systems such as that shown in figure 3. For example, the incident electric field, and therefore the induced field, produced by an electron beam passing near the intersection of two particles will be fundamentally different from the incident and induced electric field due to an electromagnetic wave, which will be homogeneous across the whole cluster. Instead, the electron beam generates a very localized electric field [27]—not unlike a SNOM probe, but an order of magnitude smaller in dimension. However, what figure 3 illustrates well is that, for this multi-particle system, the mapping of the plasmon response has allowed us to identify distinct modes associated with different kinds of resonances. In complex structures, such as mesoporous films, it is possible to map the energy of the plasmon resonance as a function of local geometry and examples of such an approach will be published elsewhere.

4. Conclusions

In summary, we have shown that EELS in the STEM can be used to measure the energy and map the distribution of surface plasmon resonances excited by a fast electron. Examples of application to gold and silver nanoparticles, singly and in clusters, were shown. These plasmon maps can be useful for correlating specific surface plasmon resonances with geometrical features on the nanometre scale and, therefore, provide a better understanding of the origin of the optical properties of small metal structures.

Acknowledgments

We gratefully acknowledge support of this work by the Australian Research Council. G A Anstis is thanked for helpful discussion.

References

[1] Nie S and Emory S R 1997 *Science* **275** 1102
[2] Kneipp K, Wang Y, Kneipp H, Perelman L T, Itzkan I, Dasari R R and Feld M S 1997 *Phys. Rev. Lett.* **78** 1667
[3] Ebbesen T W, Lezec H J, Ghaemi H F, Thio T and Wolff P A 1998 *Nature* **391** 667
[4] Barnes W L, Dereux A and Ebbesen T W 2003 *Nature* **424** 824
[5] Stockman M 2004 *Phys. Rev. Lett.* **93** 137404
[6] Hirsch L R, Stafford R J, Bankson J A, Sershen S R, Rivera B, Price R E, Hazle J D, Halas N J and West J L 2003 *Proc. Natl Acad. Sci. USA* **100** 13549
[7] Klar T, Perner M, Grosse S, von Plessen G, Spirkl W and Feldman J 1998 *Phys. Rev. Lett.* **80** 4249
[8] Ducourtieux S *et al* 2001 *Phys. Rev.* B **64** 165403
[9] Hillenbrand R and Keilmann F 2001 *Appl. Phys.* B **73** 239
[10] Bischoff M M J, van der Wielen M C M M and van Kempen H 1998 *Surf. Sci.* **400** 127
[11] Imura K, Okamoto H, Hossain M K and Kitajima M 2006 *Nano Lett.* **6** 2173
[12] Okamoto H and Imura K 2006 *J. Mater. Chem.* **16** 3920
[13] Batson P E 1980 *Solid State Commun.* **34** 477
[14] Batson P E 1982 *Phys. Rev. Lett.* **49** 936
[15] Wang Z L and Cowley J M 1987 *Ultramicroscopy* **21** 77
[16] Bosman M, Watanabe M, Alexander D T L and Keast V J 2006 *Ultramicroscopy* **106** 1024
[17] Nikoobakht B and El-Sayed M A 2003 *Chem. Mater.* **15** 1957
[18] Xu X, Stevens M and Cortie M B 2004 *Chem. Mater.* **16** 2259
[19] Haynes C L and van Duyne R P 2001 *J. Phys. Chem.* B **105** 5599
[20] Muller D A and Silcox J 1995 *Ultramicroscopy* **59** 195
[21] Jeanguillaume C and Colliex C 1989 *Ultramicroscopy* **28** 252
[22] Sönnichsen C, Franzl T, Wilk T, von Plessen G and Feldmann J 2002 *Phys. Rev. Lett.* **88** 077402
[23] Link S and El-Sayed M A 1999 *J. Phys. Chem.* B **103** 8410
[24] Draine B T and Flatau P J 1994 *J. Opt. Soc. Am.* A **11** 1491
[25] Kreibig U and Vollmer M 1995 *Optical Properties of Metal Clusters* (Berlin: Springer)
[26] Wang Z L 1996 *Micron* **27** 265
[27] Bashevoy M V, Jonsson F, Krasavin A V, Zheludev N I, Chen Y and Stockman M I 2006 *Nano Lett.* **6** 1113